ELSEVIER

Thin Solid Films 424 (2003) 15–22

thin solid films

www.elsevier.com/locate/tsf

On the island nucleation process in LPOMVPE $In_{0.2}Ga_{0.8}As/GaAs$ multilayers grown on GaAs and AlAs buffers

E. Gartstein[a,*], D. Mogilyanski[a], R. Golan[b], D. Fekete[c]

[a]*Institute for Applied Research, Ben-Gurion University, P.O. Box 653, Beer-Sheva 84105, Israel*
[b]*Department of Chemical Engineering, Ben-Gurion University, Beer-Sheva 84105, Israel*
[c]*Solid State Institute, Technion, Haifa 32000, Israel*

Abstract

A comparative study of the nucleation of In enriched islands in $In_{0.2}Ga_{0.8}As/GaAs$ multilayers grown on top of GaAs or AlAs buffers deposited on GaAs substrates with various miscut parameters was performed by using X-ray diffraction, transmission electron microscopy (TEM) and atomic force microscopy (AFM) techniques. Experimental results showed that the evolution of the self-assembly strongly depends on the miscut parameters and the morphology of the buffer/multilayer interface. For the samples with the same nominal strain misfit between the bilayers the nucleation is enhanced for the larger initial miscut on the substrate and the degree of the lateral ordering across the interface is promoted by the morphology of the underlying AlAs buffer layer.

Keywords: Nanostructured strained multilayers; Interfacial strains; X-Ray diffraction

1. Introduction

Semiconductor nanostructures have a potential for device applications. The direct growth of nanostructures based on the natural tendency of strained heteroepitaxial layers to form three-dimensional (3D) islands after formation of two-dimensional (2D) wetting layer with a thickness of a few monolayers [1] is promising apart from the processing techniques involving litography and etching. Spontaneous coherent formation of islands in lattice mismatched heteroepitaxial systems like SiGe/Si [2] InAs/GaAs [3] and other III–V and II–VI semiconductors has already been extensively studied ([4] and references therein). The islands or quantum dots (QD) imbedded into the matrix are of particular interest due to their electronic properties characteristic of zero-dimensional system. Further progress in fabrication of QD structures requires control over their formation and which requires understanding of the mechanisms governing their shape, size and arrangement. The formation of self-assembled QDs in the multilayered structures is already a recognized route to improve their uniformity and ordering [5,6]. However, the lateral ordering of the dots is controlled to a lesser extent than the vertical one. The theory invoking the relaxation of the elastic energy associated with the nucleation of the coherently strained islands was developed to explain the observed phenomena [7,8], but it is still not complete to account for morphological, thermodynamic and kinetic effects in the growth process.

$In_xGa_{1-x}As/GaAs$ system is of technological importance and the understanding of the interplay between the elastic lattice relaxation and the ordering of the nucleated islands, particularly at the initial stages is required to attain the optimal growth conditions. The microstructural model of island nucleation process was presented in the proceeding study of $Ga_{0.8}In_{0.2}As/GaAs$ multilayer composed of five bilayers grown on GaAs buffer [8]. In this model one type of the nucleated islands was described as a compositionally modulated region, where In-enriched domain was surrounded by two In depleted domains and the other one as an inclusion type with In enriched concentration. These islands nucleated on the consecutive interfaces with a

*Corresponding author. Tel.: +972-7-647-2484; fax: +972-7-67472950x2969.
E-mail address: gart@bgumail.bgu.ac.il (E. Gartstein).

0040-6090/03/$ - see front matter © 2002 Elsevier Science B.V. All rights reserved.
PII: S0040-6090(02)00898-2

skew vertical correlation. Further modifications were introduced into this model to account for the inhomogeneous In composition profile in the nucleated islands and the alternating vertical positioning on the successive interfaces [9].

In the following sections the structural features of the multilayers grown on substrates with different miscut parameters and the one grown on AlAs buffer will be compared and elaborated.

2. Experimental

The multilayered structures composed of $Ga_{0.8}In_{0.2}As/GaAs$ bilayers were grown by low-pressure organometallic vapor phase epitaxy (LPOMVPE) method in a vertical reactor using AsH_3, trimethylgallium and trimethylindium on undoped semi-insulating (001) oriented GaAs substrate (American Xtal Technology). Table 1 depicts the growth conditions for four samples with their respective code names. The supplied As/Ga ratio provided stoichiometric deposition conditions [10]. The miscut parameters of the GaAs substrates were found from X-ray measurements. To improve the surface of the substrate a buffer GaAs layer of 10 000 Å was nucleated first, followed by five bilayers $Ga_{0.8}In_{0.2}As/GaAs$ with nominal thicknesses of 50 and 100 Å, respectively, grown at the temperatures as is shown in Table 1. No evidence of misfit dislocations forming on the interfaces was observed for the thickness of the $Ga_{0.8}In_{0.2}As$ layer having a nominal misfit strain of 1.4% with GaAs. To allow direct imaging of the nucleated islands on the surface, one sample M153 was grown with three $Ga_{0.8}In_{0.2}As/GaAs$ bilayers followed by the uncapped $Ga_{0.8}In_{0.2}As$ layer with the same nominal thicknesses. AFM (Park Scientific Instruments, Autprobe CP) was used to examine their shape and positional arrangement. For sample S1445, the additional AlAs buffer layer 5000-Å thick was grown on top of the base GaAs layer. The growth of two buffers stems from the possibility of the selective etching of GaAs and AlAs layers and the possibility of using AlAs buffer for air-bridge technology. The samples were investigated by X-ray diffraction techniques employing high-resolution MRD-Philips and D^3-Bede diffractometers coupled to rotating anode generators (18 kW). The resulting thicknesses of the layers were determined from the specular θ:2θ scans in low and high angular regions with a high-resolution diffactometer in double-axis configuration followed by a numerical fit to the experimental curves. TEM study was conducted by observing cross-sectional images in a high resolution JEOL JEM-2010 electron microscope operating at 200 kV with a theoretical resolution of 1.94 Å. The cross-sectional TEM samples were prepared by a combination of mechanical polishing and Ar ion milling.

The reciprocal space maps (RSMs) of diffuse X-ray scattering (DXS) were collected in triple-axis mode in the vicinity of the various Bragg peaks. The details of the experimental results and their analysis are presented below.

3. Results

3.1. Atomic force microscopy

AFM examination of the surface morphology was carried out for the undeposited GaAs substrate and the sample M153 which was grown without the capping layer. The AFM topographs were obtained in contact mode. The GaAs substrate exhibits a step-terrace structure in the [100] miscut direction with rather irregular step edges in Fig. 1a. The nucleated islands are observed in the image of the sample M153 in Fig. 1b and for the visualization of their shape, a three-dimensional image is shown in Fig. 1d. The tendency for positional correlation of the nucleated islands on the surface is reflected by the two-dimensional Fourier transform in Table 1e from the corresponding topograph in Fig. 1b. It shows that the nucleation evolves randomly. Nevertheless, areas with certain degree of ordering of the nucleated islands were observed on the large M153 sample as can be seen in Fig. 1c and its corresponding two-dimensional Fourier transform in Fig. 1f. The positional ordering of the islands is clearly manifested by the presence of fringes close to the [110] direction and corresponding to the spacing of $\sim$570 Å between the islands. It can be also seen that the steps reorient themselves closer towards the [110] direction as compared to the image in Fig. 1b. This surface restructuring can be related to the low M153 substrate miscut of 0.3° and for the low vicinallity areas the underlying step structure is less constraining the step meandering during the deposition process. This behaviour of the growing surface evolves with the anisotropic accommodation at the different step edge directions and for the observed islands the size dimension tends to increase.

3.2. Scans in double-axis mode

The specular reflectivity θ:2θ scans measured from S1482 to S1445 multilayers and their analysis had been already presented [8]. The reflectivity showed only low amplitude fringes because of the low electron density contrast in S1482 and these became more pronounced for S1445 due to the change in the electron density introduced by the additional AlAs buffer layer. The interface roughness parameters could not be unambigiously determined from the theoretical fit for both samples.

Rocking curves and θ:2θ scans in double-axis mode produce similar patterns due to the poor detector reso-

Table 1
The growth conditions and the structural parameters of the multilayers

Sample code	Substrate miscut paramaters		Buffer thickness (Å)		Capping thickness (Å)	Actual layers thicknesses (Å)	
	Angle	Azimuth from [100] towards [110]	Growth temperature (°C)			GaAs Growth temperature (°C)	$Ga_{0.8}In_{0.2}As$
S1453	0.07°	30°±2°	GaAs (10 000) 820		125	116 650	62
S1482	2.08°	0°±2°	GaAs (10 000) 650		125	125 650	60
S1445	2.02°	11.5°±2°	GaAs (10 000) 700	AlAs (5000) 820	125	121 650	48
M153	0.34°	5°±2°	GaAs (10 000) 610		Uncapped	Thickness gradient 610	52

lution although different directions are probed in reciprocal space [11]. The measured θ:2θ scans around the symmetrical (004) substrate reflection are shown in Fig. 2 for all studied samples. The layers thicknesses for S1482 and S1445 samples refined by dynamical fitting to the superlattice (SL) peak positions in the measured curves compared well with those from the reflectivity data. The fit to the curves from samples S1453 and M153 is shown in Fig. 2 as well. The resulting average layers thicknesses T^{A}_{ave} (GaAs) and T^{B}_{ave} ($In_{0.8}Ga_{0.2}As$) are given in Table 1. It should be noted that for the investigated samples the positions of the SL peaks could be fixed by the sum of the values $\langle T^{AB}_{ave}\rangle = T^{A}_{ave} + T^{B}_{ave}$. The accurate values of uncertainty in the layers thicknesses can be determined for the samples with a higher number of bilayers. The average interplane spacing in the multilayer perpendicular to the substrate surface can be estimated from the zero SL peak (SL'0') position and compared to the one estimated as:

$$\bar{d}_{av} = T^{AB}_{ave}/(T^{A}_{ave}/d_A + T^{B}_{ave}/d_B), \quad (1)$$

where d_A and d_B are the interplane spacings of layers A and B, respectively. Concentration of In in $In_xGa_{1-x}As$ layer affects the d_B spacing and subsequently, the d_{ave}. The morphological evolution due to the redistribution of the layer constituents and due to the relaxation process in the interfacial regions cause distortion of the atomic plane spacings. This anomaly can be treated by introducing the thickness-dependent strain gradient $\partial u_z/\partial z$ which reflects the variation of the lattice constant a_z along the vertical multilayer direction in addition to the displacement field $\mathbf{u}(x,y,z)$ arising from the nucleated

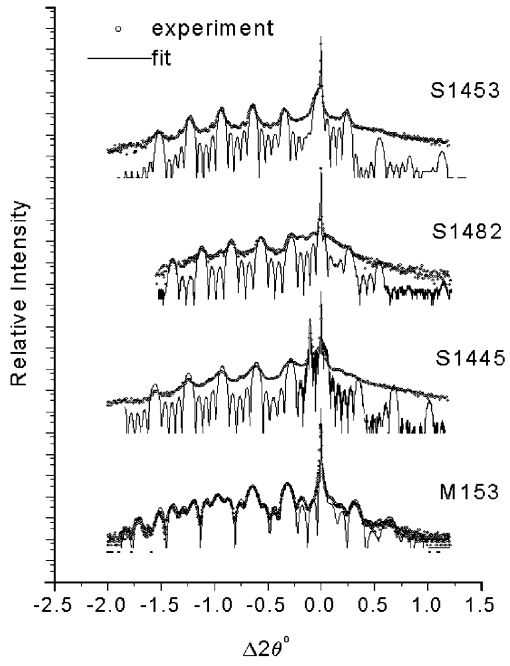

Fig. 2. The experimental and the fitted θ:2θ scans in double-axis mode for the investigated samples.

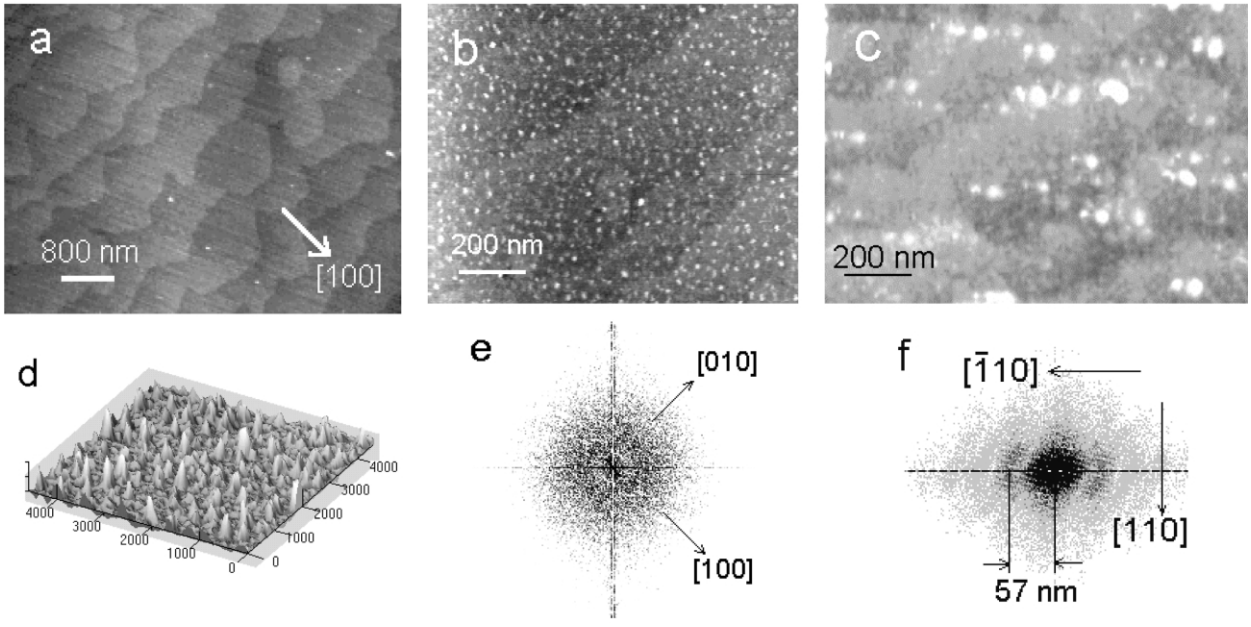

Fig. 1. AFM topographs: (a) from the surface of the virgin GaAs substrate; (b) from the uncapped sample M153 exhibiting random nucleation of the islands; (c) the same as in (b) but showing lateral ordering of the nucleated islands; (d) three-dimensional image of the nucleated islands corresponding to the one in (b); (e) two-dimensional Fourier transform corresponding to the image in (b); (f) two-dimensional Fourier transform showing side fringes corresponding to the average spacing of 570 Å between the islands in the topograph (c).

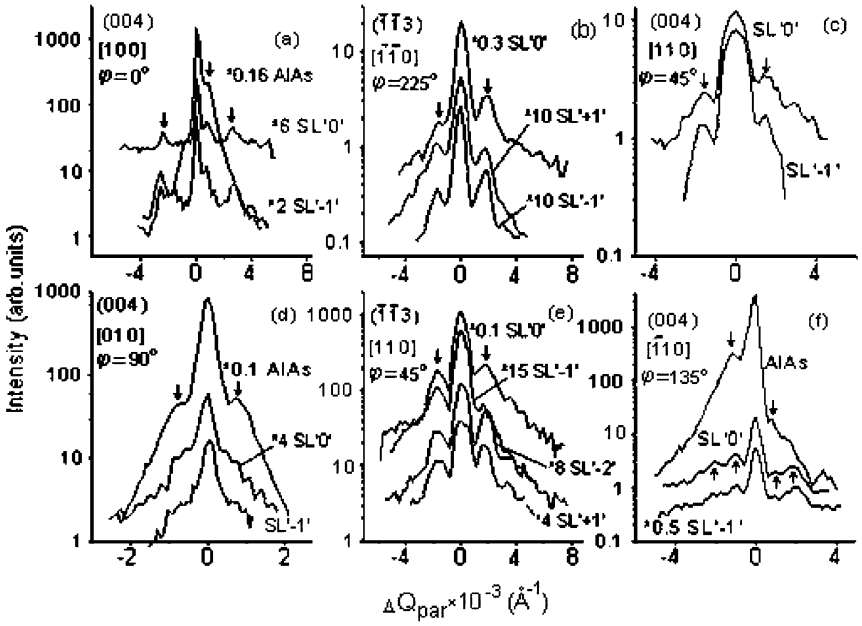

Fig. 3. (a), (b), (c), (d), (e) and (f). The experimental scans in triple-axis mode through the lateral intensity maxima at the AlAs buffer layer and the SL peaks. The scans are displaced for clarity and the multiplication factor if used is indicated. The reciprocal lattice point (HKL), the azimuthal direction on the sample surface and the relative azimuthal angle are shown in the inset. The arrows indicate the positions of the lateral intensity maxima and the corresponding correlation lenghts are given in the text.

islands [9]. Similarly, the presence of the lateral strain gradient $\partial u_x/\partial_x$ along a_x can be accounted by inhomogeneous composition in the nucleated island [9].

In a single experimental scan the effect of thickness or strain gradients might not be always obvious. However, the diffuse X-ray intensity (DXS) arising from such structural inhomogeneities is observable in RSMs near to the various substrate reflections and its analysis yields the quantitative information.

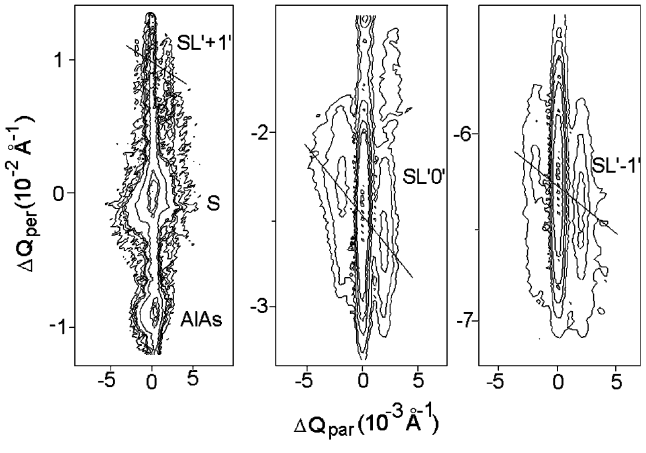

Fig. 4. (a) The RSM near to the $(\bar{1}13)$ substrate peak at $\Delta Q_{per}=0.0$ Å, AlAs buffer and SL'+1'; (b) near to the SL'0'; (c) near to the SL'−1'. The lines show the inclination of the lateral satellites with respect to the surface streak.

3.3. Scans in triple-axis mode and reciprocal space maps

The RSMs were measured for all samples. The lateral satellites arising around the SL peaks had been presented for the sample S1482 [8,9] and for the S1445, these are shown in Fig. 3, pointing to a periodic lateral patterning forming in these multilayers. Lateral satellites were not detected for S1453 and only the presence of DXS was observed for sample M153 near the azimuthal direction corresponding to the substrate miscut. The reason for these differences will be discussed below.

The vertical and lateral ordering behaviour in S1445 can be envisaged from the scans measured in triple-axis mode through the lateral intensity maxima around SL peaks of various orders in the vicinity of the substrate (004) Bragg reflections with the in-plane ⟨100⟩ or ⟨110⟩ azimuthal directions lying in the scattering plane as is shown in Fig. 3a,c,d and f, respectively. The scans measured in the vicinity of the asymmetrical $(\bar{1}13)$ reflections under grazing incidence and grazing exit conditions are shown in Fig. 3b and e with their respective azimuthal directions. In order to gain the intensity in the scans near to the higher order SL peaks the analyser window in front of the detector was relaxed for the measurement in grazing exit geometry, which also resulted in broader peaks as can be seen in Fig. 3e. Note that the scans through the lateral intensity maxima can be inclined as is depicted in Fig. 4 for the intensity

distribution map in Q_{par} and Q_{per} coordinates near to the $(\overline{1}13)$ Bragg reflection. Q_{par} and Q_{per} are the reciprocal space coordinates axes directed parallel and perpendicular to the surface of the sample, respectively.

4. Discussion

The results presented above show that the island nucleation process is not driven only by the force determined by the misfit strain, which was identical for all multilayers having the same nominal In composition and layers thicknesses, but also by the morphology determined by the substrate miscut and by the buffer layer interface affected by the diffusion characteristics of the chemically different adatoms. The RSMs measured at high Bragg angle peaks did not reveal lateral satellites for S1453 having a negligible substrate miscut as well as for M153 with a substrate miscut of 0.34° apart from the weak DXS. Nevertheless, for the latter sample the AFM examination showed the appearance of the randomly nucleated islands on the uncapped $In_{0.2}Ga_{0.8}As$ surface and also regions with laterally ordered islands in the [110] direction. For both S1482 and S1445 samples the lateral satellites around SL peaks in RSMs were observed pointing to the islands positional ordering along the interfaces.

4.1. On the wetting layer formation

The presented above dynamical fitting to the scans in Fig. 1 could be achieved by fixing the average bilayer thickness $\langle T_{ave}^{AB} \rangle$ and by letting the ratio between the layers thicknesses T_{ave}^{A} and T_{ave}^{B} bilayers. For samples S1453 and S1445 this ratio was practically constant, whereas decrease of the GaAs layer thickness (or increase of the $In_{0.2}Ga_{0.8}As$ layer thickness) from the first to the last bilayer with an overall change of 6 Å (two–three monolayers) had to be introduced for S1482. The scan for the M153 sample depicted in Fig. 1 exhibits noticeable shoulders around the SL peaks, which become more pronounced with the increasing SL order. A good fit in Fig. 1 could be achieved when a gradient in thicknesses of the GaAs spacer layers was introduced, while the thickness of the $In_{0.2}Ga_{0.8}As$ layers remained close to the nominal one given in Table 1. Interestingly, the agreement with the experiment could be achieved by either increasing or decreasing the thickness gradient and not by varying the In composition in the layers. The gradient with the GaAs layer thicknesses decreasing from the bottom towards the surface with an overall change of 26 Å (~10 monolayers) seems to be more physically viable, partly because the GaAs layer can expand vertically more than the elasticity theory predicts due to the coherency strains at the interfaces and due to the wetting layer (WL) formation upon deposition of $In_{0.2}Ga_{0.8}As$ layer which becomes conformable with GaAs, thus increasing its thickness at the low interfaces and decreasing at the upper ones where the nucleation of the islands is intensified according to AFM observations. Similar redistribution behavior of the material between the WL and the islands was found in TEM study of five bilayers stack in Si/Ge system [12] and in InAs/GaAs system as well [13]. The decrease in the thickness of the WL was attributed to the strain fields evolving in the multilayer. Thus, the thickness of the spacer layer will be a factor biasing the planar growth in stacked layers gradually reducing WL thickness as more material accumulates in the nucleated islands. In the presented simulations, this phenomenon was not considered since it is difficult to account for the varying fractional coverage, although it can be invoked to explain the experimental results.

The wetting thickness effects are less pronounced for the S1482 sample due to the higher miscut of the substrate which disrupts the coherency from the start of deposition. At stepped surfaces resulting from high miscut angle the growth of deposited monolayers proceeds via wetting at the steps. Due to the finite terrace width the continuous wetting layer is expected to break up into domains [14]. The wetting is even more prohibited in S1445 sample due to the AlAs buffer layer morphological roughening in different azimuthal directions as well as to its effect on the directional lateral migration of the atoms.

4.2. Vertical and lateral ordering

Available reports in the literature suggest a vertical correlation for $In_xGa_{1-x}As/GaAs$ or SiGe/Si systems [5,15–17], whereas in this study a vertical anticorrelational order evolves between the three low interfaces and the two successive ones as has resulted from the simulations of RSMs [8,9] and cross-sectional TEM observation shown in Fig. 5. It is also claimed that the lateral ordering tendency is most effective for materials with inclined layer-to-layer stackings, which is dependent on the elastic anisotropy of the material and the spacer layer thickness.

The RSMs for S1482 sample had been already presented [8,9]. Lateral patterning in this sample gives rise to satellites near to the SL peaks. For S1482 the lateral ordering dimensions are ~2500 and ~3600 Å in [100] and [110] directions, respectively, and these relate as $\sim\sqrt{2}$, while no correlations were observed in both respective directions at 90°. The scans measured in triple-axis mode along ⟨100⟩ and ⟨110⟩ directions from the sample S1445 are depicted in Fig. 3. It should be noted that the scans are performed through the AlAs buffer peak or the SL peaks by crossing the adjacent lateral maxima. These lateral maxima can be inclined with respect to the streak perpendicular to the surface of the sample as has been mentioned above. The

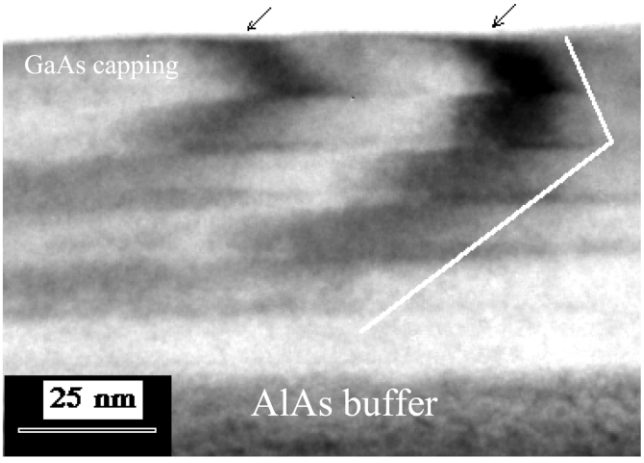

Fig. 5. Cross-sectional TEM image of S1445 sample viewed along [110] direction. The white lines indicate the vertical skew positioning of the islands on the interfaces. The arrows show the undulation dip on the top surface above the islands.

correlation distance $L_{cor}=2\pi/\Delta Q_{par}$ between the islands is determined by the position of the lateral satellites. A pair of lateral satellites is observed in Fig. 3a around the SL peaks along the [100] direction to which azimuthal angle of 0° is ascribed. The magnitude of L_{cor} along the interfaces in this direction is ~2500 Å. It can be also noticed that the satellite maxima are asymmetric with respect to ΔQ_{par}. The reason for such asymmetry was shown to result from the inhomogeneous In composition in the islands and also due to their vertical skew positioning [9]. Additional lateral peak with a spacing of −8500 Å is present in both scans through the SL peaks and in the scan through the AlAs buffer peak. It should be pointed out that the strain field due to the nucleated islands is exerted into the underlying buffer layer. Calculations accounting for this strain field in the buffer showed that its contribution to the intensity of the satellite near to the buffer is relatively smaller than the one observed in the measurements [8]. It was also shown by the simulations that the strain caused by the step morphology can significantly contribute to the satellite near to the buffer peak [9]. The DXS in RSMs at high Bragg angles although being not sensitive to the morphological shape of the structural feature unless its dimensions are significant, does depend on the strain field associated with it. Therefore, it is likely that the satellite near the buffer peak is due to the evolved AlAs morphology which is replicated into the overlayers upon deposition and aids to reduce the nucleation energy in the strain driven island formation process. The off-specular DXS measurements near to the zero Bragg peak will help to clarify the interfacial morphological structure in this multilayer [18].

The scans measured along the [010] azimuth exhibit significantly less pronounced lateral satellites, although in the scan through the AlAs peak the shoulders corresponding to the morphological perturbations with spacing of ~8500 Å can be clearly observed. The weaker satellites around the SL peaks point to a lower degree of lateral correlation and/or larger dimensions of the islands along the [010] azimuth.

The experimental scans across the lateral satellites along the $[\bar{1}10]$ and [110] azimuthal directions are shown in Fig. 3b and e near to the (113) substrate reflection under grazing incidence and grazing exit diffraction conditions, respectively, and near to the (004) reflection in Fig. 3c. The pair of satellites observed in these scans corresponds to the lateral spacing of ~3500 Å, which relates by $\sim\sqrt{2}$ to the spacing along the [100] direction. Such a relation was also observed for the S1482 sample. It is interesting to note that the azimuthal difference for the scans shown in [3]b and e is 180°. The intensity of the lateral satellites is reversed upon azimuthal rotation of 180° for a symmetrical reflection like (004) or asymmetrical reflection measured under the same incidence or exit diffraction when the satellites are caused by the strain associated with the structural features of morphological origin. As can be seen in Fig. 3b,e there is no reversal in the satellites intensities because the measurements are made at the same reciprocal lattice point by changing the grazing incidence geometry to the one with grazing exit. The evolving morphology at the interfaces and the strain field in the multilayer are strongly interrelated.

The scan through the AlAs buffer peak along the [110] azimuthal direction exhibits a lateral satellite at a negative ΔQ_{par} corresponding to a spacing of −6500 Å and another one at a positive ΔQ_{par} corresponding to a spacing of ~8500 Å. These satellites are appearing in the scans through the SL′0′ and SL′-1′ peaks as well. The azimuth of the miscut for S1445 sample is between [100] and [110] directions (see Table 1), therefore, it is likely that these lateral satellites originate from the growth morphology of the AlAs buffer, which replicates into the deposited layers. The experiments show that the evolution of the morphological features differs along [110] and $[\bar{1}10]$ interface directions. A plausible reason for the differences along [110] and $[\bar{1}10]$ stems from the different diffusion rates in the two ⟨110⟩ directions known to produce anisotropic growth of the epilayers [19]. The ordering of the nucleated islands emerging along the [110] interfacial direction is manifested by another pair of lateral satellites in the scans through the SL peaks with a correlation length of ~3000 Å.

5. Summary

The vertical and lateral ordering of the islands in the upper layers is affected by the strain introduced by low layers. In addition, it is biased by the initial substrate morphology defined by the miscut parameters as well

as the morphology evolving on the buffer layer, being dependent on its chemical composition. Formation of the island on the top of the wetting layer depends on the nucleation free energy, which is modulated by the aforementioned factors and, therefore, is governed by the total built-up strain configuration in the multilayer. The minimum in the strain energy has to be sufficient for the island nucleation to occur.

These conclusions follow from the findings in this study of the substrate miscut effect on the three-dimensional nucleation process. The islands evolve along both ⟨100⟩ and ⟨110⟩ interface directions in the multilayer grown on AlAs buffer, whereas for the one grown on GaAs layer these were found to be confined to [100] and [110] directions. These differences are evidently imposed by the lateral morphology of the grown AlAs buffer. Referring to the morphological study of the AlAs/GaAs multilayer grown on GaAs substrate with similar miscut parameters employing X-ray offspecular measurements near to the zero Bragg peak along various interfacial directions it was observed that morphological perturbations develop along both ⟨110⟩ directions and thus, can serve as the nucleation centers for the islands [18].

References

[1] J.H. Merwe, Interface Sci. 6 (1998) 225.
[2] Y.W. Mo, D.E. Savage, B.S. Schwartzentruber, M.G. Lagally, Phys. Rev. Lett. 65 (1990) 1020.
[3] L. Goldstein, F. Glas, J.Y. Marzin, M.N. Charasse, G. Le Roux, Appl. Phys. Lett. 47 (1985) 1099.
[4] D. Bimberg, M. Grundmann, N.N. Ledentsov, Quantum Dot Heterostructures, Wiley, Chichester, 1998.
[5] J. Tersoff, C. Teichert, M.G. Lagally, Phys. Rev. Lett. 76 (1996) 1675.
[6] G. Springholz, M. Pinczolits, V. Holy, S. Zerlauth, I. Vavra, G. Bauer, Phys. E 9 (2001) 149.
[7] V. Holy, G. Springholz, M. Pinczolits, G. Bauer, Phys. Rev. Lett. 83 (1999) 356.
[8] D. Mogilyanski, E. Gartstein, M. Blumin, D. Fekete, R. Kohler, J. Phys. D: Appl. Phys. 34 (2001) A19.
[9] D. Mogilyanski, E. Gartstein, J. Cryst. Growth 324 (2002) 646.
[10] A. Shen, Y. Horikoshi, H. Ohno, S. Guo, Appl. Phys. Lett. 71 (1977) 1540.
[11] D. Mogilyanski, M. Blumin, E. Gartstein, R. Opitz, R. Kohler, J. Cryst. Growth 198/199 (1999) 1070.
[12] O.G. Schmidt, O. Kienzle, Y. Hao, K. Ebert, F. Ernest, Appl. Phys. Lett. 74 (1999) 1272.
[13] S. Rouvimov, Z. Liliental-Weber, W. Swider, J. Washburn, E.R. Weber, A. Sasaki, A. Wakahara, Y. Furkawa, T. Abe, S. Noda, J. Electron. Mater. 27 (5) (1998) 427.
[14] K. Binder, in: M.G. Lagally (Ed.), Kinetics of Ordering and Growth at Surfaces, Vol. 239, of NATO Advanced Study Institute, Series B:Physics, Plenum, New-York, 1990.
[15] Q. Xie, A. Madhukar, P. Chen, N. Kobayashi, Phys. Rev. Lett. 75 (1995) 2542.
[16] G.S. Solomon, J.A. Trezza, A.F. Marshall, J.S. Harris Jr., Phys. Rev. Lett. 76 (1996) 952.
[17] W. Wu, J.R. Tucker, J.S. Harris Jr., Appl. Phys. Lett. 71 (1997) 1083.
[18] D. Mogilianski, E. Gartstein, M. Blumin, D. Fekete, R. Opitz, R. Kohler, J. Phys. D:Appl. Phys. 32 (1999) A239–A244.
[19] H. Lee, J.A. Johnson, P.M. Petroff, J. Vac. Sci. Technol. B 18 (2000) 2193.